Bioconjugate Chemistry

pubs.acs.org/bc

Article

Interconversion of Unexpected Thiol States Affects the Stability, Structure, and Dynamics of Antibody Engineered for Site-Specific Conjugation

Carolina T. Orozco, Matthew J. Edgeworth, Paul W. A. Devine, Alistair R. Hines, Owen Cornwell, Christopher Thompson, Xiangyang Wang, Jonathan J. Phillips, Peter Ravn, Sophie E. Jackson, and Nicholas J. Bond*

Cite This: *Bioconjugate Chem.* 2021, 32, 1834−1844

Read Online

ACCESS | Metrics & More | Article Recommendations | Supporting Information

ABSTRACT: Antibody−drug conjugates have become one of the most actively developed classes of drugs in recent years. Their great potential comes from combining the strengths of large and small molecule therapeutics: the exquisite specificity of antibodies and the highly potent nature of cytotoxic compounds. More recently, the approach of engineering antibody−drug conjugate scaffolds to achieve highly controlled drug to antibody ratios has focused on substituting or inserting cysteines to facilitate site-specific conjugation. Herein, we characterize an antibody scaffold engineered with an inserted cysteine that formed an unexpected disulfide bridge during manufacture. A combination of mass spectrometry and biophysical techniques have been used to understand how the additional disulfide bridge forms, interconverts, and changes the stability and structural dynamics of the antibody intermediate. This quantitative and structurally resolved model of the local and global changes in structure and dynamics associated with the engineering and subsequent disulfide-bonded variant can assist future engineering strategies.

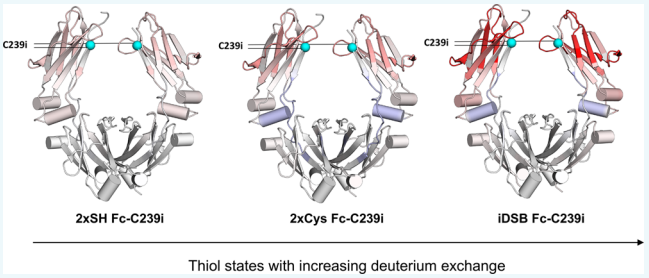

INTRODUCTION

Antibody−drug conjugates (ADCs) have become very promising therapeutics in oncology by combining the high specificity of a tumor-recognizing monoclonal antibody (mAb) with the potency of a chemotherapeutic small molecule (payload).[1] Combining two therapeutic molecules into a single agent reduces the systemic toxicity of small molecule chemotherapy while facilitating the use of more potent cytotoxic agents which, if administered alone, would have significant dose limitation due to toxicity.[2−6] ADCs represent a huge area of research, with currently nine FDA-approved ADCs on the market, including five within the past year, and more than 60 ADCs are being clinically evaluated in more than 200 active or recently completed clinical trials[7] (Clinicaltrials.gov). In the first generation of ADCs, the payload was conjugated to lysines, which led to a distribution in number and position of drugs attached, resulting in variable drug-to-antibody ratios (DARs).[8] The DAR is an important contributor to the therapeutic index: the dose range within which efficacy is achieved with an acceptable safety profile and must be tightly controlled. To do this, the field has iterated toward the conjugation of payloads to canonical cysteines and then to strategies that enabled site-specific conjugation, including non-natural amino acids,[9−11] the use of enzymes such as formylglycine generating enzyme,[12] transglutaminase[13,14] and sortase A,[15] as well as point mutations to add unpaired cysteines for conjugation, either by substitution[16] or by insertion.[17] In particular, the addition of a cysteine near the hinge region of an IgG1 scaffold has been investigated,[16−18] and both the substitution at position 239 (Eu mAb numbering) in the heavy chain (S239C) and the insertion after that position (C239i) have given promising results:[16,17] both cysteines are easily conjugated, provide stability of the payload over time, decrease FcγR binding, and do not affect the binding to the neonatal Fc receptor (FcRn), which should ensure a half-life similar to that of the wild-type scaffold.[16,17]

During large-scale manufacture (50−500 L) of several C239i antibodies, we observed that the inserted cysteine could adopt three distinguishable chemical states. Using nonreduced peptide mapping, these were characterized as free thiol (2xSH), capped with cysteine (cysteinylated, 2xCys, forming commonly on free cysteines in an oxidizing environment where cysteines are present in the media;[19] this is a common

Received: May 28, 2021
Revised: July 2, 2021
Published: August 9, 2021

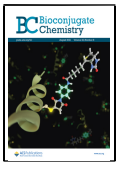

modification during manufacturing), or forming an additional disulfide bridge between both C239i residues (iDSB) (Figure S1 and Figure 1). A fourth state, 1xCys + 1xSH (containing both free thiol and cysteinylated C239i), was also observed, although in much smaller proportions. Further analysis revealed that the proportions of these different thiol states vary from lot to lot and across different antibodies (Figure S2A). Interestingly, oxidized thiol states (2xCys and iDSB) predominate during expression in Chinese hamster ovarian (CHO) cells under fed-batch culture (Figure S2B), and it is upon harvest that reduced forms are introduced: 2xSH and 1xCys + 1xSH. The thiol state appears to be largely unaffected by the subsequent purification steps (Figure S2C), and while the proportion of iDSB appears to vary between antibodies and from lot-to-lot, the iDSB was invariably present.

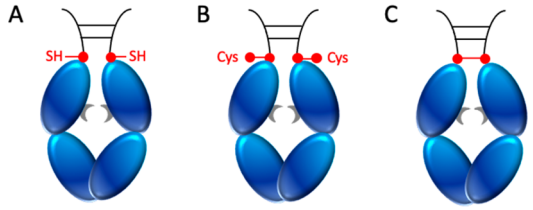

Figure 1. Schematic of the Fc domain containing the inserted cysteine after position 239 (Fc-C239i), in the three predominant forms: (A) free thiol (2xSH), (B) doubly cysteinylated (2xCys), and (C) forming an additional disulfide bridge between both C239i residues (iDSB). Drawn in gray: glycosylation. A partially cysteinylated state, 1xCys + 1xSH (containing both free thiol and cysteinylated C239i), was also observed during manufacture, although in much smaller proportions and was not enriched for further characterization.

The additional disulfide bridge (iDSB) was confirmed by tandem mass spectrometry (MS/MS) to be an additional interchain disulfide bond between the two inserted cysteines, downstream of the two canonical disulfide bonds that covalently bond IgG1 heavy chains; no evidence of scrambling was observed (Figure S3 and Supporting Information section 4.1). The presence of the additional interchain disulfide bridge is surprising since the α-carbons of the amino acids at position 239 on each heavy chain are 17.2 Å apart from each other in the crystal structure (PDB: 3AVE), while the distance between the two α-carbons of the cysteines involved in a disulfide bridge is 6.4 Å (canonical disulfide bridges in 3AVE). This raises questions regarding how the iDSB forms and the resulting structural changes necessary to accommodate it.

In this study, we investigate in detail the structural consequences of inserting cysteine at position C239i and the associated thiol states observed during manufacture of the antibody intermediate. To investigate this systematically, Fc constructs enriched for each of the three thiol states were generated (2xSH, 2xCys, and iDSB Fc-C239i), verified, and quantified by mass spectrometry (Figures S4 and S5 and Table S1). The Fc constructs were used as surrogates for C239i IgG since it has been well-established that the antibody binding fragment (Fab) does not affect the stability of the C_H2 and C_H3 domains.[20,21] Chemical denaturation experiments, differential scanning calorimetry (DSC), and millisecond HDX mass spectrometry[22] were used to probe the stability, dynamics, and structures of the C_H2 and C_H3 domains in each of the enriched states. Together, these studies provide insight into the conditions under which different thiol states interconvert, their relative stabilities, and the conformational changes that occur upon formation of an additional disulfide bond. Finally, we explore the effect of iDSB on the subsequent conjugation of the antibody intermediate.

RESULTS AND DISCUSSION

Interconversion of Unexpected Thiol States. To understand how the interconversion of the thiol states can occur, conditions that could induce unfolding and increase the molecular dynamics were investigated. These stresses can be heat, low pH, shear stress, or chemical denaturation to name a few. For this study, chemical denaturant stress was selected. The evolution of the thiol states was monitored over time using nonreducing peptide mapping. Under native conditions and incubation for 7 days at 25 °C, the relative proportion of all enriched Fc variants did not change significantly (Figure 2A and Table S2). However, in the presence of chemical denaturant (3.5 M guanidinium chloride (GdmCl)), both 2xSH and 2xCys converted into the iDSB Fc-C239i (Figure 2A). Moreover, slower conversion of 2xCys to iDSB Fc-C239i was observed, suggesting that interconversion might not be direct.

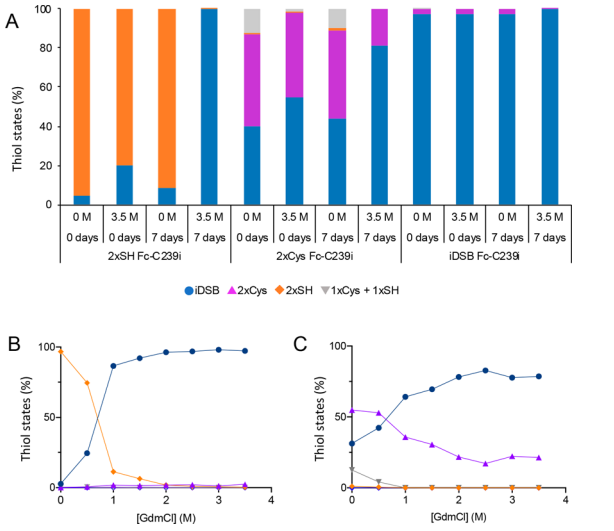

Figure 2. (A) Effect of the concentration of guanidinium chloride and incubation time at 25 °C in 20 mM His pH 5.5 on the proportion of the thiol states for each of the three initially enriched variants (2xSH, 2xCys, and iDSB Fc-C239i). (B) Effect of the concentration of denaturant after 7 days of incubation at 25 °C on 2xSH Fc-C239i and (C) 2xCys Fc-C239i enriched starting material. The error bars are too small to be visible.

To understand the interconversion in more detail, the evolution of the thiol states was monitored over a greater range of denaturant concentrations and time points, again by nonreduced peptide mapping. The conversion from 2xSH to iDSB Fc-C239i was almost complete at denaturant concentrations over 1 M GdmCl (Figure 2B and Table S3). For 2xCys Fc-C239i under equivalent conditions, the conversion to iDSB progressed but not to completion, reinforcing the hypothesis that the doubly cysteinylated form needs to convert into an intermediate, most probably the singly cysteinylated form, before converting into the iDSB (Figure 2C and Table S4). These data are further supported by the observation that rapid and relatively slow formation of iDSB from 2xSH and 2xCys Fc-C239i, respectively, occur over time at a fixed

https://doi.org/10.1021/acs.bioconjchem.1c00286
Bioconjugate Chem. 2021, 32, 1834−1844

denaturant concentration (1−4 days at 3.5 M GdmCl, Figure S6 and Tables S5 and S6).

To explain why significant interconversion only occurs in the presence of denaturant (≥1 M GdmCl), chemical denaturation unfolding experiments were performed and the thermodynamic stability of both C_H2 and C_H3 domains was determined for each of the Fc-C239i-enriched variants. The fluorescence derived from solvent-exposed tryptophan was measured after 7 days of incubation in various concentrations of GdmCl, and the data were analyzed using the average emission wavelength (AEW, eq 1) and fitted to a three-state model (eq 3). Three thermodynamic parameters were obtained: $\Delta G^{H_2O}_{X-Y}$, the difference in Gibbs free energy between two states X and Y in water; m_{X-Y}, the m value between the two states X and Y, a constant of proportionality describing how much the ΔG_{X-Y} changes upon denaturant concentration; and $[den]_{50\%\ X-Y}$, the midpoint of denaturation between states X and Y. All Fc variants showed two unfolding transitions (Figure 3A), with the first corresponding to unfolding of the C_H2 domain and the second to unfolding of the C_H3 domain.[23] Reproducibility and reversibility were demonstrated (Supporting Information section 4.2, Figures S7 and S8, and Table S9).

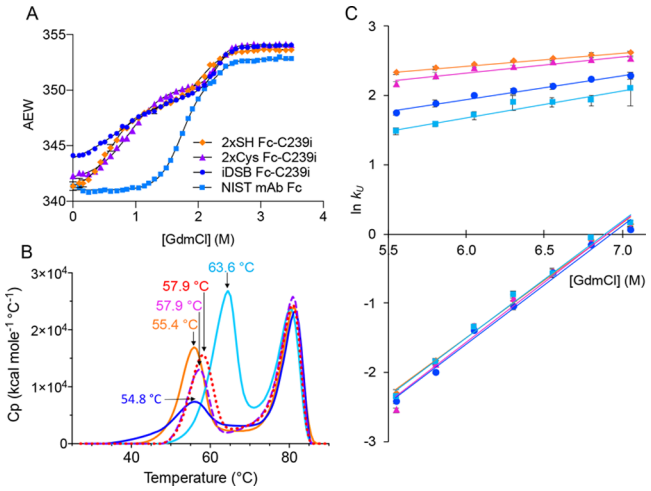

Figure 3. All biophysical experiments on the enriched variants were carried out in 20 mM His pH 5.5. (A) Unfolding curves of 2xSH Fc-C239i (orange lozenge), 2xCys Fc-C239i (purple triangles), iDSB Fc-C239i (dark blue circles), and NIST mAb Fc (light blue squares). In all cases, the values shown are the average from multiple experiments. (B) Results from DSC experiments. Thermal stabilities of 2xSH Fc-C239i (orange, solid line), 2xSH NEM-capped Fc-C239i (red, dotted line), 2xCys Fc-C239i (purple, dashed line), iDSB Fc-C239i (dark blue, solid line), and NIST mAb Fc (light blue, solid line). The experiment was performed in triplicate, but the data shown are only for one experiment. The T_m values shown are the means. For more details on the accuracy on these measurements, see Supporting Information section 4.3. (C) Unfolding kinetics 2xSH Fc-C239i (orange lozenge), 2xCys Fc-C239i (purple triangles), iDSB Fc-C239i (dark blue circles), and NIST mAb Fc (light blue squares), measured in triplicate. The fastest unfolding phases correspond to the C_H2 domain unfolding, whereas the slower unfolding phases correspond to the unfolding of the C_H3 domain. The solid line shows the best fit of the data to eq 5: $\ln k_U^{[den]} = \ln k_U^{H_2O} + m_{k_U}[den]$. Error bars represent the standard deviation from triplicate measurements. In many cases, they are not visible because they are smaller than the size of the data point.

The midpoint of denaturation observed for C_H2 domain unfolding in the 2xSH, 2xCys, and iDSB Fc-C239i were 0.58, 0.91, and 0.75 M GdmCl, respectively (Table 1). These low denaturation midpoints explain why the conversion from 2xSH and 2xCys to iDSB Fc-C239i starts to occur at 0.5 M and becomes significant over 1 M GdmCl and suggest the C_H2 domain has unfolded, at least in part, under these conditions, thereby reducing steric constraints and increasing the frequency of disulfide bond formation at the inserted cysteine.

Formation of iDSB also occurs without chemical denaturant: when 2xSH IgG-C239i was incubated at 37 °C (in 10 mM Tris, pH 8.0) for 13 days, the proportion of iDSB increased from 20 to 100%. The rate of iDSB formation increased further under heat stress with almost complete (98%) conversion after incubation at 50 °C for 24 h (Figure S9). Measurement of the thermal stability of the enriched variants by differential scanning calorimetry showed that the melting temperature of the C_H2 domain was between 54.8 and 63.6 °C (Figure 3B). Increasing the temperature may both affect the proportion of molecules that are in the denatured state (even below the T_m value) as well as increase protein dynamics and thereby potentially increase the number of local as well as global unfolding events. It is not possible to deconvolute these two effects without further experiments; therefore, it is unclear whether the iDSB forms in a fully unfolded state resulting from global unfolding of the C_H2 domain or a transiently populated partially unfolded state. What is clear is that iDSB formation occurs under physiologically relevant conditions and increases under any conditions where the stability of the native state is decreased or there has been an increase in dynamics.

A scheme for the interconversion of the different thiol states is shown in Figure 4, assuming 1xCys + 1xSH can interconvert into iDSB Fc-C239i by nucleophilic attack.[24,25]

Effect of the Cysteine Insertion on the Biophysical Stability. To determine if the thermodynamic stability of the antibody had been affected by insertion of the cysteine or the resultant thiol variants, thermodynamic parameters were measured from the chemical denaturation unfolding experiments. All enriched variants showed lower denaturation midpoints for the first transition compared to the wild-type (Table 1), suggesting that the C_H2 domain was destabilized by the insertion of the cysteine in the upper C_H2 domain. The $\Delta G^{H_2O}_{I-N}$ values demonstrate that the C_H2 domain of iDSB Fc-C239i is the least stable, followed by 2xSH Fc-C239i and finally 2xCys Fc-C239i, which are all significantly less thermodynamically stable than the wild-type (Table 1). Since the m values are correlated with the difference in solvent-accessible surface area[26] (ΔSASA) between native and denatured states, they provide useful information on the effect of the insertion on the structure. All three variants have a m_{I-N} value lower than that of the wild-type, showing that the C_H2 domain has a more solvent-accessible surface area in the native state, suggesting that conformational changes have occurred. Interestingly, the iDSB Fc-C239i has the lowest m_{I-N} value, demonstrating that either the C_H2 domain has an additional solvent-exposed surface area in the native state or that the denatured state is more structured. The midpoint of the second unfolding transition is similar for all constructs, suggesting that the stability of the C_H3 domain is unaffected by the insertion in the C_H2 domain.

DSC was employed to measure the thermal stability of the different variants. All constructs showed two unfolding transitions, the first corresponding to unfolding of the C_H2

https://doi.org/10.1021/acs.bioconjchem.1c00286
Bioconjugate Chem. 2021, 32, 1834−1844

Table 1. Thermodynamic Parameters Fitted from the Unfolding Curves[a]

proteins	m_{I-N} (kcal mol^{-1} M^{-1})	$[den]_{50\%\ I-N}$ (M)	ΔG_{I-N} (kcal mol^{-1})	m_{D-I} (kcal mol^{-1} M^{-1})	$[den]_{50\%\ D-I}$ (M)	ΔG_{D-I} (kcal mol^{-1})
2xSH Fc-C239i	2.5 ± 0.2	0.58 ± 0.02	1.5 ± 0.2	3.1 ± 0.1	2.05 ± 0.04	6.4 ± 0.3
2xCys Fc-C239i	2.099 ± 0.003	0.9060 ± 0.0001	1.902 ± 0.002	5.3 ± 0.6	2.30 ± 0.01	12 ± 1
iDSB Fc-C239i	1.3 ± 0.1	0.75 ± 0.05	1.0 ± 0.1	4.5 ± 0.2	2.272 ± 0.002	10.3 ± 0.5
NIST mAb Fc	3.2 ± 0.1	1.69 ± 0.02	5.45 ± 0.2	3.9 ± 0.5	2.25 ± 0.04	9 ± 1

[a]The values are the average of duplicate (2xCys Fc-C239i, iDSB Fc-C239i) and triplicate (2xSH Fc-C239i, NIST mAb Fc) experiments, and the error is the standard deviation of the repeats. For more details on the accuracy on these measurements, see Supporting Information section 4.2.

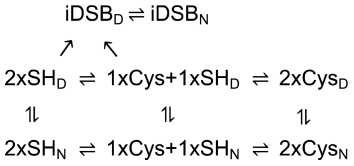

Figure 4. Interconversion network between the 2xSH, 2xCys, and iDSB Fc-C239i variants. N: C_H2 domain in the native state. D: C_H2 domain in the denatured state or with increased molecular dynamics. 2xCys can interconvert into 1xCys + 1xSH, which can interconvert into 2xSH from either the native or denatured states, and both 2xSH and 1xCys + 1xSH can interconvert into iDSB via the denatured state or with increased molecular dynamics. The 1xCys + 1xSH form could interconvert to iDSB by nucleophilic attack of the free thiol to the capped cysteine.

domain and the second to the unfolding of the C_H3 domain (Figure 3B). The thermal stability of the C_H2 domain for all Fc-C329i variants was lower than that of the wild-type, and the relative thermal stabilities were the same as those determined using chemical denaturant: iDSB < 2xSH < 2xCys < 2xSH with NEM (*N*-ethylmaleimide) < NIST mAb Fc (Figure 3B and Table S7; the NEM capping of 2xSH prevents the interconversion of 2xSH into other states). ΔH_{cal}, corresponding to the area under an unfolding peak, is a measure of the favorable interactions that must be overcome to unfold. ΔH_{cal} of the first transition for the iDSB Fc-C239i was significantly lower than all the other Fc variants and wild-type (Table S7), indicating that some favorable interactions were lost in the native state of the iDSB Fc-C239i. The peak corresponding to C_H2 unfolding was also broader for the iDSB Fc-C239i (Figure 3B), suggestive of a lower ΔC_p, which is also correlated to a lower ΔSASA.[26] This observation is consistent with the *m* value of iDSB Fc-C239i from the GdmCl experiments, suggesting that either the native state of the C_H2 domain is more solvent-accessible than that in the wild-type or that the denatured state may be more structured. The T_{m1} of Fc-C239i increased when free thiols were capped with NEM, suggesting that the apparent reduction in relative thermal stability of Fc-C239i 2xSH may be due to it converting to iDSB at elevated temperature, consistent with our previous observation (Figure S9). The melting temperatures of the C_H3 domain for all

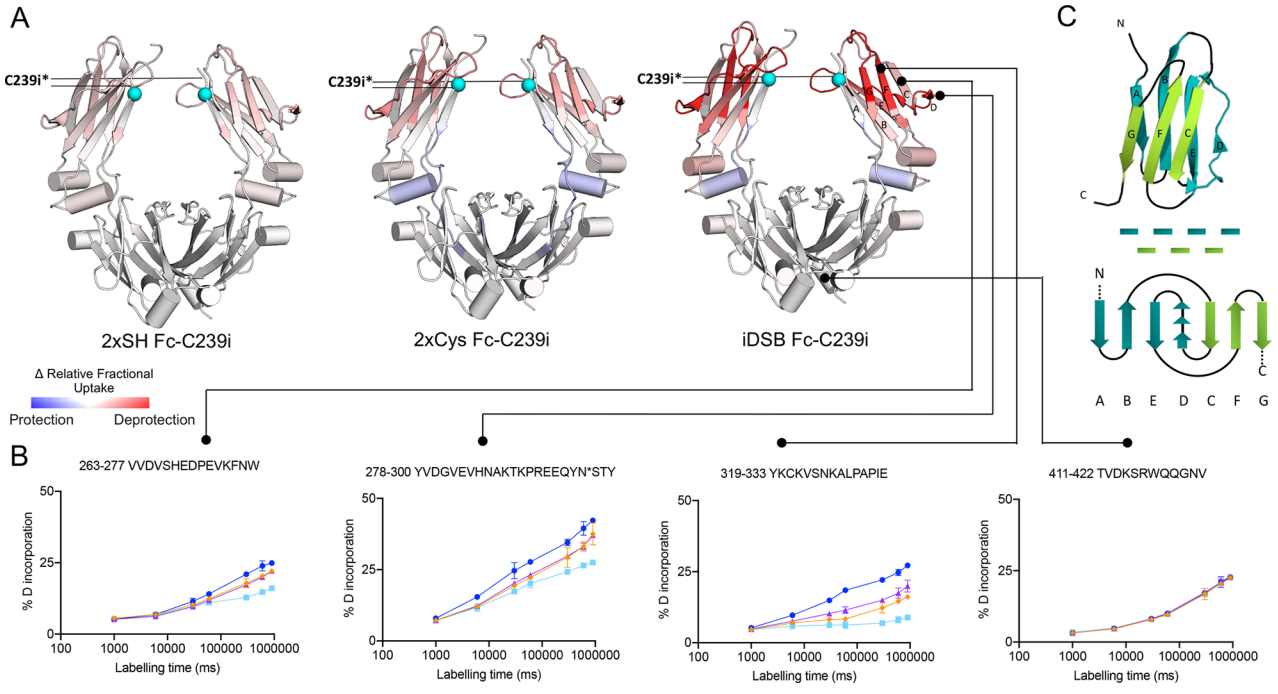

Figure 5. (A) Crystal structure (3AVE) showing the relative change in fractional deuterium exchange represented as a color scale: reduced exchange (blue), no change (white), increased exchange (red), for the three enriched Fc-C239i variants compared to wild-type and normalized to iDSB Fc-C239i. (B) Uptake plots for different regions of exchange in the Fc domain: 2xSH Fc-C239i (orange lozenge), 2xCys Fc-C239i (purple triangles), iDSB Fc-C239i (dark blue circles), and NIST mAb Fc (light blue squares). The error bars represent a Student's *t* distribution with 95% confidence interval, $n = 3$. (C) Simplified representation of the β-sandwich structure of the C_H2 domain, indicating the arrangement of the β-strands within the β-sheets and tertiary structure. *The crystal structure 3AVE corresponds to the wild-type and does not have an inserted cysteine at position 239; the annotation shows where the inserted cysteine would be located. For all uptake plots, see Figure S17.

https://doi.org/10.1021/acs.bioconjchem.1c00286
Bioconjugate Chem. 2021, 32, 1834−1844

constructs was very similar, confirming the insertion has no effect on the stability of this domain.

Unfolding kinetics provide information on the rate (and therefore frequency) at which a domain unfolds. Natively folded protein was rapidly diluted into a range of chemical denaturant concentrations, and the change in intrinsic fluorescence was measured as a proxy for protein unfolding. The data for all Fc variants (Figure 3C and Table S8) were fit with a double exponential function (eq 4) that best describes both a fast and slower unfolding phase. The unfolding rate constants of the slower phase were very similar for all variants (Figure 3C and Table S8), suggesting that this phase corresponds to the unfolding of the C_H3 domain and is in agreement with the thermodynamic stability (reported here), as well as the relative kinetic stabilities reported by Sumi and Hamaguchi.[23] The unfolding rates of the C_H2 domain for 2xSH and 2xCys Fc-C239i were very similar and faster than those of the wild-type (Figure 3C), suggesting that the insertion of a cysteine in the C_H2 domain kinetically destabilizes it. Interestingly, the rate of unfolding of iDSB was slower than the 2xSH and 2xCys Fc-C239i, indicating a higher kinetic stability. This is in contrast to the thermodynamic measurements and is likely due to the unfolding transition state being more structured than for 2xSH and 2xCys Fc-C239i. A more detailed explanation and representation are provided in Figure S11.

Effect of the Cysteine Insertion on Structural Dynamics. To investigate whether the thermodynamic and kinetic differences associated with the formation of an intramolecular disulfide bond were related to local changes in structure or dynamics, hydrogen−deuterium exchange mass spectrometry (HDX-MS) experiments were conducted. This implementation of HDX-MS uses a novel fully automated system capable of measuring hydrogen−deuterium exchange in the millisecond to minute time scale.[22] Postlabeling, online pepsin digestion was conducted and complete sequence coverage was achieved in the resulting peptide map (Figure S12). Interrogation of differences in the rate of deuterium uptake revealed that insertion of a cysteine at position 239 of the heavy chain (Fc-C239i) changes the structure and/or conformational dynamics of the C_H2 domain, which is further, and substantially, disrupted by subsequent formation of an interchain disulfide bond (Figure 5A). Significant increases (t test, p value <0.05) in deuterium exchange consistent with either increased solvent exposure and/or reduced intramolecular hydrogen bonding were observed in three locations: a small increase in exchange between residues Ser254 and Trp277 that are involved in two β-strands facing each other (strands B and C in Figure 5B,C); a larger increase in residues between Val279 and Leu306 which are in a β-strand at the edge of the β-sandwich and beginning of the next β-strand (strands D and beginning of E in Figure 5B,C); finally an increase in exchange takes place in the two last β-strands of the C_H2 domain (strands F and G, Figure 5B,C), where mixed EX1 and EX2 kinetics are observed for the iDSB (Figure 6). EX1 exchange kinetics are seldom observed and indicative of a local unfolding event. This local unfolding can be precisely localized to amino acids 319−333 in the C_H2 domain: EX1 kinetics are observed in peptide 319−348 (Figure 6) and in the shorter overlapping peptide 319−333 (Figure S15) but not in the other overlapping peptide 334−348 nor other adjacent regions. This is consistent with the conclusion that these antiparallel strands undergo local unfolding, i.e., unzipping and

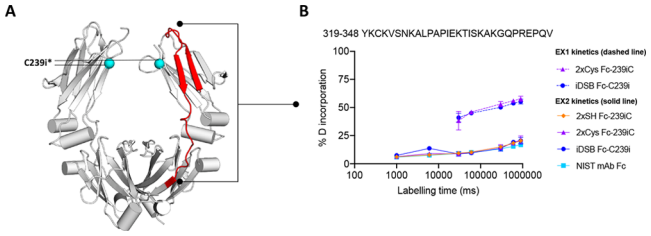

Figure 6. (A) Crystal structure of the Fc domain showing mixed EX1/EX2 kinetics in the last two β-sheets of the C_H2 domain (red on the crystal structure), peptide 319−348: YKCKVSNKALPAPIEKTISKAKGQPREPQV. Cyan spheres represent C239i. *The crystal structure 3AVE corresponds to the wild-type and does not have an inserted cysteine at position 239; the annotation shows where the inserted cysteine would be located. (B) Uptake plot representing the percentage in deuterium incorporation for the EX1 exchange (dashed line), and EX2 exchange (solid line) for the peptide 319−348 (YKCKVSNKALPAPIEKTISKAKGQPREPQV: red regions on the crystal structure).

rezipping without breaking the surrounding H-bonds of the β-sheet. The H-bonding network involved in the β-strand D has been greatly destabilized and partly broken, and the β-sheet composed of the β-strands A, B, and E has also been destabilized but to a lower extent. The mixed EX1/EX2 kinetics suggest that there is a mixed population of folded and unfolded forms of the C_H2 domain for the iDSB variant ($iDSB_D \rightleftharpoons iDSB_N$). In previous studies,[27,28] it had been observed that the β-strand G in the C_H2 domain was the most destabilized by other mutations in the C_H2 domain, demonstrating a lower stability in that specific β-strand. Modest protection was observed in the lower C_H2 domain for 2xCys and iDSB, which suggests it comes from the iDSB form (as 2xCys contains some) and not the insertion itself, potentially as a structural compensation of the distortion in the upper C_H2 domain. Overall, our data suggest that the additional disulfide bridge at the beginning of the C_H2 domain applies strain to a larger region, i.e., across the C_H2 domain, distorting it and opening it up compared to the wild-type. The 2xSH and 2xCys Fc-C239i show an increased exchange in the same regions but to a lesser extent. The C_H3 domain does not show any significant increase in deuterium exchange for any of the enriched variants when compared to the wild-type (Figure 5A,C). Gallagher et al.[18] showed by X-ray crystallography that the inserted cysteine after the 239th residue replaces the position of the serine 239 and affects the preceding residues in the hinge, resulting in a one-residue upward shift toward the N-terminus of Ser239, Pro238, and Gly237, with residues after the insertion maintaining their wild-type positions. These are rather minimal perturbations that are not consistent with their HDX-MS results. However, our more detailed HDX-MS findings are in agreement with theirs and perhaps reflect that the crystal structure may not represent the true structure in solution due to the restraints imposed by the crystal lattice.

Impact of the Additional Disulfide Bridge on the Drug to Antibody Ratio. Conjugation to an unpaired cysteine requires the functional group of the cysteine be available to react with the maleimide group of the payload's linker. It is therefore well-established that, before conjugation, the antibody has to undergo a partial reduction to remove unwanted thiol adducts, followed by a reoxidation to reform all native disulfide bridges, leaving the substituted/inserted cysteines as free thiols, available for conjugation (Figure

https://doi.org/10.1021/acs.bioconjchem.1c00286
Bioconjugate Chem. 2021, 32, 1834−1844

S16). We next investigated if the iDSB, an unexpected thiol state, can be accommodated by this routine conjugation approach in order to achieve consistent drug−antibody ratios.

For IgG-C239i, the conjugation was carried out both before and after these preparatory redox steps to compare the conjugation efficiencies. When the enriched variants were conjugated directly without reduction/reoxidation, the conjugation efficiency on 2xCys and iDSB IgG C239i was very low (Table 2). In contrast, when the partial reduction and reoxidation were carried out on the enriched variants prior to conjugation, the conjugation results showed good and consistent conjugation efficiencies resulting in DARs of 1.57, 1.54, and 1.51 for 2xSH, 2xCys, and iDSB Fc-C239i, respectively (Table 2). To understand why the empirically determined DAR was lower than the theoretical DAR of 2, the thiol states from three antibody lots were monitored by nonreduced peptide mapping in their initial state, after the reduction and reoxidation steps, and after conditions used for conjugation (but in the absence of the payload). These data demonstrate that after exposure to conditions used for reduction, reoxidation, and conjugation, some iDSB remained (∼20%) and support the hypothesis that, while consistent DAR can be achieved, iDSB formation may prevent complete conjugation to the inserted cysteines (Figure 7).

Table 2. Drug−Antibody Ratio after Conjugation of the Different Enriched Variants, Going through the Reduction/Oxidation Steps

enriched material	DAR after direct conjugation	DAR after reduction and reoxidation prior to conjugation
2xSH	1.75	1.57
2xCys	0.12	1.54
iDSB	0.08	1.51

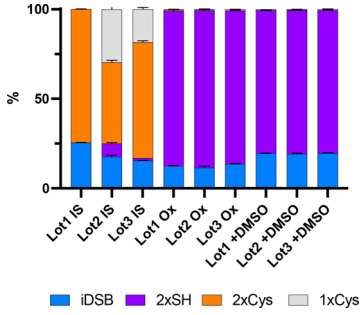

Figure 7. Proportion of thiol states in IgG-C239i monitored by nonreduced peptide mapping in their initial state (IS), after partial reduction and mild reoxidation (Ox) and after conditions used for conjugation but in the absence of the payload (DMSO). Approximately 20% of cysteines were in the iDSB state after exposure to conditions used for conjugation.

CONCLUSION

Overall, our studies demonstrate that the C_H2 domain in all the enriched variants of Fc-C239i has been destabilized by the cysteine insertion, whereas the C_H3 domain is unaffected. Previous work on antibodies containing either an insertion C239i[17] or the substitution S239C[16] showed that the thermal stability of the C_H2 domain was not affected by the substitution but was decreased by the insertion. This further demonstrates that the destabilization comes from the insertion and not from the nature of the residue. In addition to confirming that the insertion does indeed confer a modest but measurable change in structure and dynamics, here we demonstrate that a much more substantial structural perturbation can be sustained upon formation of a disulfide bond between inserted cysteines.

Herein, we have described an unexpected but naturally occurring state of the C239i mutant containing an additional disulfide bridge, the conditions under which it forms and how it affects the antibody's structure. More specifically, we showed that the three enriched Fc-C239i variants can interconvert, 2xSH and 2xCys tending toward iDSB. This happens in conditions where the two heavy chains can come close enough to form a disulfide bridge (the sulfur atoms need to be 2 Å apart[29]). This occurs during expression, and here, we demonstrated mechanistically that formation is greatly favored by conditions that either increase the molecular dynamics or the proportion of molecules where the C_H2 domain is in the denatured state. Chemical denaturant and heat were used as proxies for any stress that the antibody may experience in its lifetime, which could also be shear stress or pressure during the expression and purification steps. When this additional disulfide bridge is present, it applies an additional destabilizing strain on the C_H2 domain. The significant increase in hydrogen−deuterium exchange especially in the β-strands C, F, and G and in the β-strand D is due to H-bonding breakage and an increase in solvent-accessible surface area in the native state. This is also shown by the lower m_{I-N}, ΔC_p, and ΔH_{cal} values obtained for iDSB compared to those for 2xSH and 2xCys Fc-C239i. The change in structure of the C_H2 domain upon forming the additional interchain disulfide bridge might affect not only the native state but also the unfolding transition state, as the unfolding kinetic experiments showed that the iDSB Fc-C239i has a kinetic stability greater than that of the other variants. All of these findings suggest that they are caused by a distortion of the C_H2 domain brought about by the formation of an additional disulfide bridge.

Our findings show that the formation and reformation (after the reduction step) of the iDSB influences the efficiency of the final conjugation step. While iDSB can be effectively reduced, its formation (∼20% in our studies) during oxidation and under conditions used for conjugation provide an explanation for a consistent but lower than anticipated DAR. This hypothesis is supported by a recent study demonstrating that iDSB contributes toward under-conjugation of the C239i antibody.[30] The same mutation and similar nearby mutations previously investigated (C239i, C238i, S239C) also produced DARs lower than 2 (1.8, 1.44, and 1.9, respectively[17]). This work highlights the importance of systematic studies on iDSB formation for cysteine engineered antibodies in order to fine-tune conditions to achieve desired conjugation efficiencies. Despite the iDSB formation, these data also demonstrate that the C239i scaffold can be consistently conjugated to achieve a DAR similar to those observed for comparable constructs.

Taken together, these data demonstrate the utility of combining biophysical techniques with high-resolution mass spectrometry to provide detailed characterization of the structure and dynamics of biopharmaceuticals and their variants. Similar observations are anticipated for other engineered antibodies where cysteines are introduced close to the hinge, and the insight provided here serves to guide future cysteine or site-specific engineering strategies.

https://doi.org/10.1021/acs.bioconjchem.1c00286
Bioconjugate Chem. 2021, 32, 1834−1844

EXPERIMENTAL SECTION

Antibody Expression and Purification. The antibodies used in this study were NIST mAb Fc, the control protein, and Fc-C239i, a construct described in Dimasi et al.,[17] with the exact same amino acid sequence as NIST mAb but with a cysteine inserted at position 239 in the C_H2 domain. All antibodies were produced at AstraZeneca. The gene for the human Fc-C239i (Dimasi et al., 2017) was cloned into a mammalian expression vector. The Fc-C239i protein was transiently expressed in Chinese hamster ovary cells under serum-free conditions. Cleared culture supernatant was loaded directly onto MabSelect SuRe column equilibrated with PBS (pH 7.2). Fc-C239i was eluted with 0.1 M glycine pH 2.7. Pooled fractions were buffer exchanged into PBS.

Measurement of the Thiol States of Fc-C239i-Enriched Variants in Specific Denaturant Concentrations and Incubation Times. *Sample Preparation.* For each of the three variants, 100 μg was prepared in 34 μL, in 0 or 3.5 M GdmCl, in 20 mM His pH 5.5. They were incubated for 0 or 7 days at 25 °C.

Nonreduced Peptide Map Preparation: NEM Capping, Denaturation, and Lys-C Digestion. After the incubation, the samples were alkylated by adding 5 μg of NEM and incubated at room temperature for 20 min. Samples were then buffer exchanged three times into 7.1 M GdmCl, 5.6 mM phosphate pH 7.0, and 0.1 M NaCl with 10 kDa Amicon filters and concentrated to a final volume of 90 μL. Next, 250 μL of 100 mM phosphate buffer pH 7.0, 1 μL of 40 mM EDTA, and 10 μL of 1 mg/mL of endoproteinase Lys-C were added to each sample and incubated for 2 h at 37 °C. Ten microliters at 1 mg/mL of Lys-C were added again and incubated for another 2 h at 37 °C. After digestion, the material was split in half. Five microliters of 500 mM dithiothreitol (DTT) were added to 45 μL of digested protein and incubated at room temperature to reduce. Five microliters of water were added to 45 μL of the same sample to act as a nonreduced control. Both samples were run side by side by LC-MS for comparative analysis.

LC-MS Run. The digested samples were analyzed by means of reverse-phase liquid chromatography (Acquity i-Class UPLC, Waters, Manchester, UK) coupled to mass spectrometry (Orbitrap Fusion ThermoFisher mass spectrometer). Reduced and nonreduced samples were compared to identify disulfide-containing peptides, and identification was performed using a combination of MS1 and MS2. Peptides were separated using a Peptide BEH C18 column, 300 Å 1.7 μm, 2.1 mm × 150 mm (Waters, Manchester, UK) over a 76 min linear gradient of 5−45% B (mobile phase A: 0.02% TFA in water; mobile phase B: 0.02% TFA in ACN). MS data were acquired over a 250−2000 m/z range, using an AGC target of 200000 and a maximum injection time of 50 ms. MS2 was acquired in the ion trap in centroid mode, using an AGC target of 10000 and a maximum injection time of 35 ms. Fragmentation was achieved by collision-induced dissociation using a collision energy of 35%. The data were then processed on the Qual Browser Thermo Xcalibur 3.0.63 software.

Mass Spectrometry Data Analysis. The peptides corresponding to the hinge region were searched (NEM-capped, cysteine-capped, and disulfide bridged). The presence of the variants was quantitated by combining the most intense isotope on the 4+ m/z and 5+ m/z distribution and then integrating the area under the obtained peaks on the total ion count chromatogram.

Results are shown in Figure 2A and Table S2.

Evolution of the Thiol States of Fc-C239i-Enriched Variants over Time and upon Increasing Denaturant Concentrations. *Sample Preparation.* The first set of experiments consisted of observing the effect of denaturant concentration after 7 days of incubation at 25 °C on the inserted cysteine states. For this first set of experiments, 100 μg of the free-thiol-enriched and doubly capped cysteine-enriched variants were prepared in 0, 0.5, 1, 1.5, 2, 2.5, 3, and 3.5 M GdmCl, in 20 mM His pH 5.5 in 34 μL total. They were incubated 7 days at 25 °C.

The second set of experiments aimed at assessing the effect of incubation time at 25 °C in 3.5 M GdmCl on the inserted-cysteine states. For the second set of experiments, 100 μg of the free-thiol-enriched and doubly capped cysteine-enriched variants were prepared 3.5 M GdmCl, in 20 mM His pH 5.5 in 34 μL total. They were incubated for 0, 1, 2, 3, and 4 days at 25 °C.

Nonreduced Peptide Map Preparation: NEM Capping, Denaturation, and Lys-C Digestion. After the incubation, the samples were alkylated adding 5 μg of NEM, and incubated at room temperature for 20 min. The samples were buffer exchanged three times into 7.1 M GdmCl, 5.6 mM sodium phosphate pH 7.0 and 0.1 M NaCl with 10 kDa Amicon filters, concentrated to a final volume of 60 μL, and incubated at 37 °C for 30 min. From this volume, 15 μL was taken (25 μg of antibody) and was then diluted by 4 in 100 mM $NaPO_4$ pH 7.0 containing 0.4% 40 mM EDTA, diluting the guanidinium chloride concentration to 1.8 M in preparation for digest. An aliquot of 10 μL (0.5 μg) of Lys-C was added to ∼25 μg of thiol-capped denatured protein at a 1:50 enzyme/protein ratio, and the mixture was incubated at 37 °C for 2 h. A further 10 μL (0.5 μg) of Lys-C was added and incubated for a final 2 h. Samples were then analyzed.

Reversed-Phase LC. Mobile phase A contained 0.1% TFA in water, and mobile phase B contained 0.1% TFA in 100% acetonitrile. The following LC conditions were used: flow rate 0.15 mL/min, column temperature 55 °C throughout the separation with the autosampler maintained at 4 °C. Injections of 10 μL of 0.42 mg/mL peptide sample were separated using a UPLC peptide CSH C18, 130 Å pore size, 1.7 μm bead size, 2.1 mm × 150 mm column (Acquity). The gradient started at 0% B until a step up to 24% at 4 min and then gradually increased to 26% at 8 min, followed by a step up to 80%. The gradient was dropped back to 100% A to equilibrate for the next injection. Total run time per samples was 12 min.

Mass Spectrometer Settings. On a Waters Xevo TQS, the MS desolvation temperature was 600 °C, and source cone voltage was 40 V, with desolvation gas flow of 400 L/h, capillary voltage of 3 kV, and Q3 collision energy of 40 eV. The different variants were targeted according to the values referenced in Table 3.

Results are shown in Figure 2B and Figure S6.

Table 3. Chromatographic and m/z Parameters for the Identification of the Variants

compound	RT (min)	m/z precursor ion	m/z fragment ion
iDSB	5.70 ± 0.20	1416.50	566.30
2xCys	5.50 ± 0.20	1476.70	566.30
1xSH + 1Cys	6.20 ± 0.22	1478.20	566.30
2xSH	8.00 ± 0.30	1479.70	566.30

https://doi.org/10.1021/acs.bioconjchem.1c00286
Bioconjugate Chem. 2021, 32, 1834−1844

Measurement of the Thermodynamic Stability of the Antibodies: Chemical Unfolding and Refolding Curves. *Methods.* Chemical unfolding and refolding curves in guanidinium chloride were performed in duplicate or triplicate. Each experiment was composed of 41 points (120 μL total volume) of increasing concentrations of GdmCl from 0 to 3.5 or 4 M final concentration. Next, 110 μL of denaturant solution was mixed with 10 μL of protein to a final concentration of 1 μM. For the unfolding curves, the stock protein solution was made in 20 mM histidine buffer pH 5.5; for the refolding curves, the protein was first denatured in 5 M GdmCl for 15 min at room temperature and then dispensed into the same 41 point denaturant solutions. The solutions were dispensed with a liquid handling robot (Microlab500 Series, ML541C, Hamilton Company). The denaturant solutions mixed with the protein were incubated at 25 °C at different time points until they reached equilibrium (7 days). Each of the 41 denaturation points was measured in a 100 μL quartz cuvette (Hellma, Precision Cell in Quartz SUPRASIL, type no. 105.250-QS, light path: 10 × 2 mm, center: 20 mm). The fluorescence was recorded with a Cary 400 Eclipse fluorescence spectrophotometer (Agilent Technologies) thermostated at 25 °C controlled by a heat block. The samples were excited at 280 nm, and the emission was recorded from 300 to 400 nm, with a scan rate of 300 nm min^{-1}; excitation and emission band passes were set at 10 nm.

Data Analysis. When the protein is denatured with increasing concentrations of chemical denaturant, the maximum of the fluorescence signal shifts toward red wavelengths. In the native state, the wavelength of maximum fluorescence intensity is at approximately 335 nm, and in the denatured state, the wavelength of maximum fluorescence is around 360 nm. The data were analyzed using an average emission wavelength (AEW), which is the arithmetic mean of the wavelengths weighted by the fluorescence intensity at each wavelength. It is calculated as shown in eq 1:

$$\mathrm{AEW} = \frac{\sum_{i=1}^{N} F_i \cdot \lambda_i}{\sum_{i=1}^{N} F_i} \tag{1}$$

where F_i is the intensity of fluorescence at the wavelength i and λ_i is the wavelength.

A three-state model in which an intermediate state between the native and denatured state is sufficiently stable to be populated and observed was used. The equilibrium between the different species is as follows:

$$\mathrm{N} \underset{K_{\mathrm{I-N}}}{\rightleftharpoons} \mathrm{I} \underset{K_{\mathrm{D-I}}}{\rightleftharpoons} \mathrm{D} \tag{2}$$

The denaturation curves, using the AEW data, were fitted to a three-state model using eq 3:[31,32]

$$F = \frac{\alpha_N + \beta_N \cdot [\mathrm{den}] + \alpha_I \cdot \exp\left(\frac{m_{\mathrm{I-N}}}{RT} \cdot ([\mathrm{den}] - [\mathrm{den}]_{50\%\,\mathrm{I-N}})\right) + (\alpha_D + \beta_D \cdot [\mathrm{den}]) \exp\left(\frac{m_{\mathrm{I-N}}}{RT} \cdot ([\mathrm{den}] - [\mathrm{den}]_{50\%\,\mathrm{I-N}})\right) \exp\left(\frac{m_{\mathrm{D-I}}}{RT} \cdot ([\mathrm{den}] - [\mathrm{den}]_{50\%\,\mathrm{D-I}})\right)}{1 + \exp\left(\frac{m_{\mathrm{I-N}}}{RT} \cdot ([\mathrm{den}] - [\mathrm{den}]_{50\%\,\mathrm{I-N}})\right) + \exp\left(\frac{m_{\mathrm{I-N}}}{RT} \cdot ([\mathrm{den}] - [\mathrm{den}]_{50\%\,\mathrm{I-N}})\right) \exp\left(\frac{m_{\mathrm{D-I}}}{RT} \cdot ([\mathrm{den}] - [\mathrm{den}]_{50\%\,\mathrm{D-I}})\right)} \tag{3}$$

where α_N, α_I, and α_D are the fluorescence of the native, intermediate, and denatured states in H_2O, respectively; β_N, β_I, and β_D are the slopes of native, intermediate, and denatured baselines, respectively; $m_{\mathrm{I-N}}$ and $m_{\mathrm{D-I}}$ are the m values between the intermediate and native state, and denatured and intermediate states, respectively; $\Delta G^{H_2O}_{\mathrm{I-N}}$, $\Delta G^{H_2O}_{\mathrm{D-I}}$, and $\Delta G^{H_2O}_{\mathrm{D-N}}$ are the differences in Gibbs free energy between the intermediate and native states, denatured and intermediate states, and denatured and native states, respectively; T is the temperature, and R is the gas constant.

Measurement of the Thermal Stability of the Antibodies: Differential Scanning Calorimetry. *Methods.* The thermal denaturation of NIST mAb Fc, 2xSH Fc-C239i, 2xCys Fc-C239i, iDSB Fc C239i, as well as 2xSH capped by NEM to avoid interconversion of the cysteine state during the thermal denaturation was monitored by differential scanning calorimetry in triplicate (duplicates for 2xSH NEM capped Fc-C239i), with a Malvern MicroCal VP-DSC instrument. Five hundred microliters of protein at 0.5−5 mg mL^{-1} in 20 mM histidine pH 5.5 was used for each run. For each protein, the baseline was measured first, which consists of buffer in both cells (buffer versus buffer), and then the protein was run (buffer versus protein). Several cleanup cycles with water and suitability controls with lysozyme at 3 mg mL $^{-1}$ in water were employed before and after the actual experiment with the antibody. Each protein sample was scanned twice to investigate the thermal reversibility. The temperature was ramped from 25 to 100 °C, increasing by 95 °C h^{-1}. The prescan thermostat was set to 2 min, and no postscan thermostat was employed. All of the different protein constructs were run in triplicate. The thermal unfolding is not reversible, as the trace of the reheated sample did not overlap with the initial one (Figure S10).

Data Analysis. The data were processed with the Origin version 7.0 SR4 software. The baseline thermogram (buffer versus buffer) was subtracted from the thermogram of the protein (buffer versus protein). Two baselines, one at the beginning and one at the end of the thermogram, were placed to adjust the data, which was then normalized using the concentration of the protein. The unfolding peaks were selected, and the thermogram was fitted to the "Non 2-state" model to obtain the melting temperatures (T_m) and the enthalpy of unfolding at the T_m, ΔH_{cal}.

Measurement of the Kinetic Stability of the Antibodies: Unfolding Kinetics. *Methods.* For the stopped-flow experiments, the native protein and the denaturant solutions were mixed in a 1:10 ratio, respectively. Seven stock solutions of guanidinium chloride (GdmCl) were prepared in 20 mM histidine buffer pH 5.5 so that the final concentrations range from 5.5 to 7.0 M GdmCl with an interval of 0.25 M. The stock solutions are 1.1-fold more concentrated than the final solutions, as solutions were diluted by a factor of 10/11 in the rapid mixing step. The protein stock solutions were prepared between 7 and 11 μM to achieve a final concentration between 0.5 and 1 μM after mixing with the denaturant solutions.

The unfolding kinetics were monitored with a SX20 stopped-flow spectrometer from Applied Photophysics (software: SX Spectrometer Control Panel Application version 2.2.27). The temperature of the water bath was set to 25 °C; the excitation wavelength was set to 280 nm, and both slit widths were 2 mm. A cutoff filter of 320 nm was used. Three short time traces were recorded with pressure hold (2 s) to

https://doi.org/10.1021/acs.bioconjchem.1c00286
Bioconjugate Chem. 2021, 32, 1834−1844

accurately measure the fastest unfolding phase, and three longer time traces (120 s) were acquired to accurately measure the slower unfolding phase, both at each denaturant concentration.

Fitting of Unfolding Kinetics. The unfolding curves were fitted with the software Pro DataViewer version 4.2.27. The fluorescence signal corresponding to the unfolding was fitted with a double-exponential function (eq 4).

$$A(t) = A_1 \cdot \exp(-k_1 t) + A_2 \cdot \exp(-k_2 t) + c \quad (4)$$

where A_1 and A_2 are the amplitudes, k_1 and k_2 the respective unfolding rate constants, and c is the offset.

The natural logarithm of the rate constants was then calculated and plotted versus the corresponding denaturant concentration, and the data fitted with eq 5.[33]

$$\ln k_U^{[den]} = \ln k_U^{H_2O} + m_{k_U}[den] \quad (5)$$

where $k_U^{[den]}$ is the observed unfolding rate constant at the denaturant concentration [den], $k_U^{H_2O}$ is the unfolding rate constant in water, and m_{k_U} is the slope of the plot of ln $k_U^{[den]}$ versus denaturant concentration.

Fast Hydrogen–Deuterium Exchange Mass Spectrometry. The peptide map was done on the 2xCys-enriched Fc-239iC variant, with equilibration buffer (20 mM His pH 5.5 in H_2O), using a data-dependent acquisition (DDA) MS^2 approach. MS data were acquired in the Orbitrap Fusion (ThermoFisher) over a 300−2000 m/z range, using an AGC target of 200000 and a maximum injection time of 100 ms. MS2 was acquired in the ion trap in centroid mode, using an AGC target of 10000 and a maximum injection time of 35 ms. Fragmentation was achieved by HCD using a collision energy of 30%. The labeled data on the three enriched variants 2xSH, 2xCys, iDSB Fc-C239i, and the wild-type NIST mAb Fc were recorded after 1000, 6000, 30000, 60000, 300000, 600000, and 900000 ms of incubation at 20 °C in deuterated buffer (in 20 mM His pD 5.5 in D_2O) with a MS1 method (300−2000 m/z range, AGC target of 200000 and maximum injection time of 100 ms) to avoid scrambling of the deuterations. All data points were run in triplicate.

On the ms2 min HDX system[22] (patent WO2020074863A1), 10 μL of protein at 5 μM in equilibration buffer (20 mM His pH 5.5 in H_2O) was diluted 20-fold at 20 °C into equilibration or labeling buffer (20 mM His pH 5.1 (pD 5.5) in D_2O) to generate a peptide map or labeled data, respectively. The mixture was then diluted 1:1 with quench buffer at 2 °C (100 mM His, 8 M urea, 0.5 M TCEP, pH 2.5). The quench solution was then injected into a Waters nanoAcquity UPLC system, flowing for 4 min at 50 μL/min onto the pepsin column at 20 °C for digestion (Waters Enzymate BEH pepsin column (2.1 × 30 mm, 5 μm)) to the trap column (Acquity UPLC BEH C18 1.7 μm column P/N 186003975; pushed by LC-MS grade H_2O with 0.2% formic acid) and then eluting from the C18 analytical column (Acquity UPLC BEH C18 1.7 μm 1.0 × 100 mm column P/N 186002346) for 10 min, from a 5 to 40% organic phase (ACN with 0.2% formic acid).

The peptide map was generated on BioPharmaFinder from equilibration data (in 20 mM His pH 5.5 in H_2O) acquired with a MS2 method. The peptides obtained were filtered by the MS identification method (MS2 only), and the peptide mass error was lower than 10 ppm. The exported csv with the peptides as well as that same undeuterated data was imported into HDExaminer to operate a second filtration of the peptides: only the charge state with the highest intensity from the peptide map data was kept per peptide for comparative accuracy between the charge states, selected according the highest intensity, the sharpest extracted ion chromatogram. After the peptide pool was curated, the labeled data were added, and the D incorporation per peptide data was then exported as a csv file. Given that the N-terminus of the Fc domain was different for the wild-type NIST mAb Fc and the Fc-C239i variants, the first peptides do not exist for the wild-type, and the data comparison starts at residue Lys 242. We employed two complementary methods of analysis to identify which deuterium incorporations were significant to observe the deuterium exchange for each time point separately and overall.

The data processing method used was first described by Dobson et al.[34] Starting with a csv file containing the D incorporation data, this Matlab-coded method first assesses if the incorporation of deuterium per peptide is significant compared to the wild-type (assessed by a t test, if p value <0.05) and then sums the significant time points per peptide, subsequently converts the peptide D incorporation to amino acid incorporation by dividing the D incorporation by the maximal number of D that can be exchanged per peptide, subtracting the D incorporation from the wild-type, and dividing the amino acid incorporation by the redundancy and finally normalizing it. The output is the deuterium incorporation for each individual amino acid. The crystal structure of the Fc domain (PDB: 3AVE) was colored with the red-white-blue scale according to the relative incorporation of deuterium per amino. The additional cysteine was removed from the incorporation data to map on the structure. The differential plots obtained are presented in Figure S13, and the summary HDX-MS parameters are in Table S10. A second method, developped by Cornwell et al.[35] was used and discussed in Supporting Information section 1.4.

Conjugation Conditions. Two conjugations processes were used to evaluate the effect the thiol state of the inserted cysteine had on the DAR or the effect the conjugation process had on the thiol state. The antibodies were conjugated to a tubulysin payload via a maleimide-bearing mc-Lys protease cleavable linker. Antibody intermediate samples were conjugated directly by spiking preparations with excess payload and providing sufficient time for the conjugation to complete. Alternatively, the antibody intermediate was reduced and reoxidized prior to conjugation. Reduction was achieved using TCEP, which was subsequently removed with 3× buffer exchange steps (10× dilution and reconcentration using 30 kDa amicon spin filters) prior to reoxidizing in dhAA. All reactions were performed at room temperature, with excess reactants and sufficient time to allow the reactions to complete.

DAR Measurement by RP-HPLC. Each sample was normalized to 2 mg/mL in HPLC water. Fifty microliters of denaturing buffer (8 M guanidine HCl, 160 mM Tris, 1 mM EDTA, pH 7.6) and 2 μL of DTT were added to 50 μL of each sample and incubated at 37 °C for 30 min. Ten microliters of each sample was injected onto a Waters BioResolve RP mAb polyphenyl column (2.1 × 150 mm, 2.7 μm, 450 Å). Mobile phase A consisted of 0.1% TFA and water, and mobile phase B consisted of 0.1% TFA in acetonitrile. A gradient of 32.5 to 46.5% mobile phase B was run from 2 to 30 min at a flow rate of 0.5 mL/min. The eluted protein was detected by UV absorbance at a wavelength of 280 nm. DAR and drug-load distribution were calculated based on peak areas.

https://doi.org/10.1021/acs.bioconjchem.1c00286
Bioconjugate Chem. 2021, 32, 1834−1844

■ ASSOCIATED CONTENT

Supporting Information

The Supporting Information is available free of charge at https://pubs.acs.org/doi/10.1021/acs.bioconjchem.1c00286.

Additional results and methods, Figures S1−S16, and Tables S1−S10 (PDF)

■ AUTHOR INFORMATION

Corresponding Author

Nicholas J. Bond − *Analytical Sciences, Biopharmaceutical Development, R&D, AstraZeneca, CB21 6GH Cambridge, United Kingdom;* orcid.org/0000-0002-0312-7360; Email: nick.bond@astrazeneca.com

Authors

Carolina T. Orozco − *Yusuf Hamied Department of Chemistry, University of Cambridge, CB2 1EW Cambridge, United Kingdom;* orcid.org/0000-0001-7274-8833

Matthew J. Edgeworth − *Analytical Sciences, Biopharmaceutical Development, R&D, AstraZeneca, CB21 6GH Cambridge, United Kingdom*

Paul W. A. Devine − *Analytical Sciences, Biopharmaceutical Development, R&D, AstraZeneca, CB21 6GH Cambridge, United Kingdom*

Alistair R. Hines − *Analytical Sciences, Biopharmaceutical Development, R&D, AstraZeneca, CB21 6GH Cambridge, United Kingdom*

Owen Cornwell − *Analytical Sciences, Biopharmaceutical Development, R&D, AstraZeneca, CB21 6GH Cambridge, United Kingdom*

Christopher Thompson − *Purification Process Sciences, Biopharmaceutical Development, R&D, AstraZeneca, Gaithersburg, Maryland 20878, United States*

Xiangyang Wang − *Analytical Sciences, Biopharmaceutical Development, R&D, AstraZeneca, Gaithersburg, Maryland 20878, United States*

Jonathan J. Phillips − *Living Systems Institute, Department of Biosciences, University of Exeter, EX4 4QD Exeter, United Kingdom;* orcid.org/0000-0002-5361-9582

Peter Ravn − *Antibody Discovery and Protein Engineering, R&D, AstraZeneca, CB21 6GH Cambridge, United Kingdom*

Sophie E. Jackson − *Yusuf Hamied Department of Chemistry, University of Cambridge, CB2 1EW Cambridge, United Kingdom*

Complete contact information is available at: https://pubs.acs.org/10.1021/acs.bioconjchem.1c00286

Author Contributions

The manuscript was written through contributions of all authors. All authors have given approval to the final version of the manuscript.

Notes

The authors declare no competing financial interest.

■ ACKNOWLEDGMENTS

This work was supported by AstraZeneca and the Engineering and Physical Sciences Research Council Centre for Doctoral Training in Sensor Technologies and Applications under Grant EP/L015889/1.

■ ABBREVIATIONS

ADC, antibody−drug conjugate; mAb, monoclonal antibody; DAR, drug to antibody to ratio; C239i, scaffold with inserted cysteine after position 239; FcRn, neonatal Fc receptor; iDSB, interchain disulfide bridge; 2xSH, free thiol; 2xCys, capped with cysteine or cysteinylated; CHO, Chinese hamster ovary; GdmCl, guanidinium chloride; HDX-MS, hydrogen−deuterium exchange mass spectrometry; DSC, differential scanning calorimetry; NEM, *N*-ethylmaleimide

■ REFERENCES

(1) Gébleux, R., and Casi, G. (2016) Antibody-Drug Conjugates: Current Status and Future Perspectives. *Pharmacol. Ther. 167*, 48−59.

(2) Alley, S. C., Zhang, X., Okeley, N. M., Anderson, M., Law, C.-L., Senter, P. D., and Benjamin, D. R. (2009) The Pharmacologic Basis for Antibody-Auristatin Conjugate Activity. *J. Pharmacol. Exp. Ther. 330*, 932−938.

(3) Lutz, R. J., and Whiteman, K. R. (2009) Antibody-Maytansinoid Conjugates for the Treatment of Myeloma. *MAbs 1*, 548−551.

(4) Ikeda, H., Hideshima, T., Lutz, R. J., Yasui, H., Okawa, Y., Kiziltepe, T., Vallet, S., Pozzi, S., Santo, L., Perrone, G., et al. (2008) The Monoclonal Antibody NBT062 Conjugated to Cytotoxic Maytansinoids Has Selective Cytotoxicity Against CD138-Positive Multiple Myeloma Cells In Vitro and In Vivo. *Clin. Cancer Res. 7*, 1490−1496.

(5) Bardia, A., Mayer, I. A., Vahdat, L. T., Tolaney, S. M., Isakoff, S. J., Diamond, J. R., O'Shaughnessy, J., Moroose, R. L., Santin, A. D., Abramson, V. G., et al. (2019) Sacituzumab Govitecan-Hziy in Refractory Metastatic Triple-Negative Breast Cancer. *N. Engl. J. Med. 380*, 741−751.

(6) Modi, S., Saura, C., Yamashita, T., Park, Y. H., Kim, S.-B., Tamura, K., Andre, F., Iwata, H., Ito, Y., Tsurutani, J., et al. (2020) Trastuzumab Deruxtecan in Previously Treated HER2-Positive Breast Cancer. *N. Engl. J. Med. 382*, 610−621.

(7) Birrer, M. J., Moore, K. N., Betella, I., and Bates, R. C. (2019) Antibody-Drug Conjugate-Based Therapeutics: State of the Science. *JNCI J. Natl. Cancer Inst. 111*, 538−549.

(8) Beck, A., Goetsch, L., Dumontet, C., and Corvaïa, N. (2017) Strategies and Challenges for the next Generation of Antibody−Drug Conjugates. *Nat. Rev. Drug Discovery 16*, 315−337.

(9) Kim, C. H., Axup, J. Y., and Schultz, P. G. (2013) Protein Conjugation with Genetically Encoded Unnatural Amino Acids. *Curr. Opin. Chem. Biol. 17*, 412−419.

(10) Lang, K., and Chin, J. W. (2014) Cellular Incorporation of Unnatural Amino Acids and Bioorthogonal Labeling of Proteins. *Chem. Rev. 114*, 4764−4806.

(11) Tian, F., Lu, Y., Manibusan, A., Sellers, A., Tran, H., Sun, Y., Phuong, T., Barnett, R., Hehli, B., Song, F., et al. (2014) A General Approach to Site-Specific Antibody Drug Conjugates. *Proc. Natl. Acad. Sci. U. S. A. 111*, 1766−1771.

(12) Rabuka, D., Rush, J. S., deHart, G. W., Wu, P., and Bertozzi, C. R. (2012) Site-Specific Chemical Protein Conjugation Using Genetically Encoded Aldehyde Tags. *Nat. Protoc. 7*, 1052−1067.

(13) Jeger, S., Zimmermann, K., Blanc, A., Grünberg, J., Honer, M., Hunziker, P., Struthers, H., and Schibli, R. (2010) Site-Specific and Stoichiometric Modification of Antibodies by Bacterial Transglutaminase. *Angew. Chem., Int. Ed. 49*, 9995−9997.

(14) Strop, P., Liu, S.-H., Dorywalska, M., Delaria, K., Dushin, R. G., Tran, T.-T., Ho, W.-H., Farias, S., Casas, M. G., Abdiche, Y., et al. (2013) Location Matters: Site of Conjugation Modulates Stability and Pharmacokinetics of Antibody Drug Conjugates. *Chem. Biol. 20*, 161−167.

(15) Madej, M. P., Coia, G., Williams, C. C., Caine, J. M., Pearce, L. A., Attwood, R., Bartone, N. A., Dolezal, O., Nisbet, R. M., Nuttall, S. D., et al. (2012) Engineering of an Anti-Epidermal Growth Factor Receptor Antibody to Single Chain Format and Labeling by Sortase A-Mediated Protein Ligation. *Biotechnol. Bioeng. 109*, 1461−1470.

(16) Thompson, P., Fleming, R., Bezabeh, B., Huang, F., Mao, S., Chen, C., Harper, J., Zhong, H., Gao, X., Yu, X.-Q., et al. (2016) Rational Design, Biophysical and Biological Characterization of Site-Specific Antibody-Tubulysin Conjugates with Improved Stability, Efficacy and Pharmacokinetics. *J. Controlled Release 236*, 100−116.
(17) Dimasi, N., Fleming, R., Zhong, H., Bezabeh, B., Kinneer, K., Christie, R. J., Fazenbaker, C., Wu, H., and Gao, C. (2017) Efficient Preparation of Site-Specific Antibody−Drug Conjugates Using Cysteine Insertion. *Mol. Pharmaceutics 14*, 1501−1516.
(18) Gallagher, D. T., McCullough, C., Brinson, R. G., Ahn, J., Marino, J. P., and Dimasi, N. (2019) Structure and Dynamics of a Site-Specific Labeled Fc Fragment with Altered Effector Functions. *Pharmaceutics 11*, 546.
(19) Raju, T. S. Cysteinylation of Proteins. *Co- and Post-Translational Modifications of Therapeutic Antibodies and Proteins*; John Wiley & Sons, Inc.: Hoboken, NJ, 2019; pp 35−38.
(20) Wu, H., Kroe-Barrett, R., Singh, S., Robinson, A. S., and Roberts, C. J. (2014) Competing Aggregation Pathways for Monoclonal Antibodies. *FEBS Lett. 588*, 936−941.
(21) Ionescu, R. M., Vlasak, J., Price, C., and Kirchmeier, M. (2008) Contribution of Variable Domains to the Stability of Humanized IgG1Monoclonal Antibodies. *J. Pharm. Sci. 97*, 1414−1426.
(22) Kish, M., Smith, V., Subramanian, S., Vollmer, F., Lethbridge, N., Cole, L., Bond, N. J., and Phillips, J. J. Allosteric Regulation of Glycogen Phosphorylase Solution Phase Structural Dynamics at High Spatial Resolution. *bioRxiv* 2019, https://doi.org/10.1101/654665.
(23) Sumi, A., and Hamaguchi, K. (1982) Denaturation by Guanidine Hydrochloride of the Fc(t) and PFc' Fragments of Human Immunoglobulin G. *J. Biochem. 92*, 823−833.
(24) Alegre-Cebollada, J., Kosuri, P., Rivas-Pardo, J. A., and Fernández, J. M. (2011) Direct Observation of Disulfide Isomerization in a Single Protein. *Nat. Chem. 3*, 882−887.
(25) Gilbert, H. F. (1995) Thiol/Disulfide Exchange Equilibria and Disulfidebond Stability. *Methods Enzymol. 251*, 8−28.
(26) Myers, J. K., Pace, C. N., and Scholtz, J. M. (1995) Denaturant m Values and Heat Capacity Changes: Relation to Changes in Accessible Surface Areas of Protein Unfolding. *Protein Sci. 4*, 2138−2148.
(27) Edgeworth, M. J., Phillips, J. J., Lowe, D. C., Kippen, A. D., Higazi, D. R., and Scrivens, J. H. (2015) Global and Local Conformation of Human IgG Antibody Variants Rationalizes Loss of Thermodynamic Stability. *Angew. Chem., Int. Ed. 54*, 15156−15159.
(28) Walters, B. T., Jensen, P. F., Larraillet, V., Lin, K., Patapoff, T., Schlothauer, T., Rand, K. D., and Zhang, J. (2016) Conformational Destabilization of Immunoglobulin G Increases the Low PH Binding Affinity with the Neonatal Fc Receptor. *J. Biol. Chem. 291*, 1817−1825.
(29) Bhattacharyya, R., Pal, D., and Chakrabarti, P. (2004) Disulfide Bonds, Their Stereospecific Environment and Conservation in Protein Structures. *Protein Eng., Des. Sel. 17*, 795−808.
(30) Cao, M., De Mel, N., Jiao, Y., Howard, J., Parthemore, C., Korman, S., Thompson, C., Wendeler, M., and Liu, D. (2019) Site-Specific Antibody-Drug Conjugate Heterogeneity Characterization and Heterogeneity Root Cause Analysis. *MAbs 11*, 1064−1076.
(31) Scholtz, J. M., Grimsley, G. R., and Pace, C. N. (2009) Solvent Denaturation of Proteins and Interpretations of the m Value. *Methods Enzymol. 466*, 549−565.
(32) Gani, K., Bhambure, R., Deulgaonkar, P., Mehta, D., and Kamble, M. (2020) Understanding Unfolding and Refolding of the Antibody Fragment (Fab). I. In-Vitro Study. *Biochem. Eng. J. 164*, 107764.
(33) Jackson, S. E., and Fersht, A. R. (1991) Folding of Chymotrypsin Inhibitor 2. 1. Evidence for a Two-State Transition. *Biochemistry 30*, 10428−10435.
(34) Dobson, C. L., Devine, P. W. A., Phillips, J. J., Higazi, D. R., Lloyd, C., Popovic, B., Arnold, J., Buchanan, A., Lewis, A., Goodman, J., et al. (2016) Engineering the Surface Properties of a Human Monoclonal Antibody Prevents Self-Association and Rapid Clearance in Vivo. *Sci. Rep. 6*, 38644.
(35) Cornwell, O., Radford, S. E., Ashcroft, A. E., and Ault, J. R. (2018) Comparing Hydrogen Deuterium Exchange and Fast Photochemical Oxidation of Proteins: a Structural Characterisation of Wild-Type and ΔN6 β2-Microglobulin. *J. Am. Soc. Mass Spectrom. 29*, 2413−2426.

https://doi.org/10.1021/acs.bioconjchem.1c00286
Bioconjugate Chem. 2021, 32, 1834−1844